THE JOURNAL OF PHYSICAL CHEMISTRY C
A JOURNAL OF THE AMERICAN CHEMICAL SOCIETY

pubs.acs.org/JPCC

Article

3R-TaS_2 as an Intercalation-Dependent Electrified Interface for Hydrogen Reduction and Oxidation Reactions

Hamid Ghorbani Shiraz,* Zia Ullah Khan, Daniel Péré, Xianjie Liu, Yannick Coppel, Mats Fahlman, Magnus Berggren, Radoslaw Chmielowski, Myrtil L. Kahn, Mikhail Vagin,* and Xavier Crispin

Cite This: *J. Phys. Chem. C* 2022, 126, 17056−17065

Read Online

ACCESS | Metrics & More | Article Recommendations | Supporting Information

ABSTRACT: Hydrogen technology, as a future breakthrough for the energy industry, has been defined as an environmentally friendly, renewable, and high-power energy carrier. The green production of hydrogen, which mainly relies on electrocatalysts, is limited by the high cost and/or the performance of the catalytic system. Recently, studies have been conducted in search of bifunctional electrocatalysts accelerating both the hydrogen evolution reaction (HER) and the hydrogen oxidation reaction (HOR). Herein, we report the investigation of the high efficiency bifunctional electrocatalyst TaS_2 for both the HER and the HOR along with the asymmetric effect of inhibition by organic intercalation. The linear organic agent, to boost the electron donor property and to ease the process of intercalation, provides a higher interlayer gap in the tandem structure of utilized nanosheets. XRD and XPS data reveal an increase in the interlayer distance of 22%. The HER and the HOR were characterized in a Pt group metal-free electrochemical system. The pristine sample shows a low overpotential of −0.016 V at the onset. The intercalated sample demonstrates a large shift in its performance for the HER. It is revealed that the intercalation is a potential key strategy for tuning the performance of this family of catalysts. The inhibition of the HER by intercalation is considered as the increase in the operational window of a water-based electrolyte on a negative electrode, which is relevant to technologies of electrochemical energy storage.

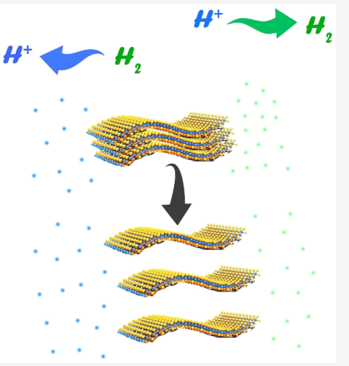

INTRODUCTION

For many decades, hydrogen has been identified as a key energy carrier for a sustainable future society, as it offers a high energy density and principally no negative direct impact on the environment, with respect to CO_2 emissions. Hydrogen generation, as a first step toward a hydrogen economy, has been a matter of debate among scientists. Although many production methods, like photochemical or cracking reformation, or gasification of biomass, are being operated all over the world, there are several problems with current methods such as low yield or major environmental impacts.

One of the most efficient and clean processes to produce hydrogen is via an electrochemical hydrogen evolution reaction (HER). There are many electrocatalysts for the HER that possesses high efficiencies, among which Pt, Rh, and Pd[1,2] are commonly considered and explored. Although numerous candidates like hybrid structures (core−shell, alloys, composites, etc.),[3,4] doped atom systems,[5] metal organic frameworks,[6] metal oxide arrays,[7] etc. have shown proper performance characteristics, several major problems still lie ahead. Several studies are being conducted in the search for a cost-effective (especially targeting platinum group metal-free catalysts), efficient, and scalable electrocatalyst. In that context, transition metal dichalcogenides (TMDs) constitute another class of two-dimensional materials where the elemental periodic unit is composed of an atomic layer of a transition metal (Ti, Ta, Mo, W, etc.) in the center with a chalcogen atomic layer (S, Se) on either side. The geometry of chalcogen atoms with respect to transition metal results in various crystal structures (1T, 2H, 3R, etc.) where T, H, and R represent overall structures (trigonal, hexagonal, and rhombohedral) and symmetry repetition is given with the number (1, 2, 3) of layers.[8] TMDs like WS_2 display significant activity for the HER.[9] Also, MoS_2 is one of the most investigated TMDs toward the HER.[10−12] Among TMDs, tantalum disulfide (TaS_2) exhibits the highest temperature-dependent electronic conductivity,[13−15] which motivates the investigation of the HER electrocatalytic activity of this 2D material (see Figure 1a and b). It is demonstrated that the majority of 2D structures is catalytically several times more active at the edge sites, as compared to the basal plane.[16] To improve the (electro)-catalytic activity, several modifications with the aim of activation of TaS_2 sheets are studied, such as plasma treatment,[17] chemical exfoliation,[18] atom-scale dispersion,[19,20] interfacial engineering, etc. Yu et al. have been using theoretical

Received: June 21, 2022
Revised: September 20, 2022
Published: September 29, 2022

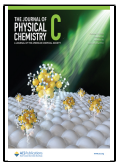

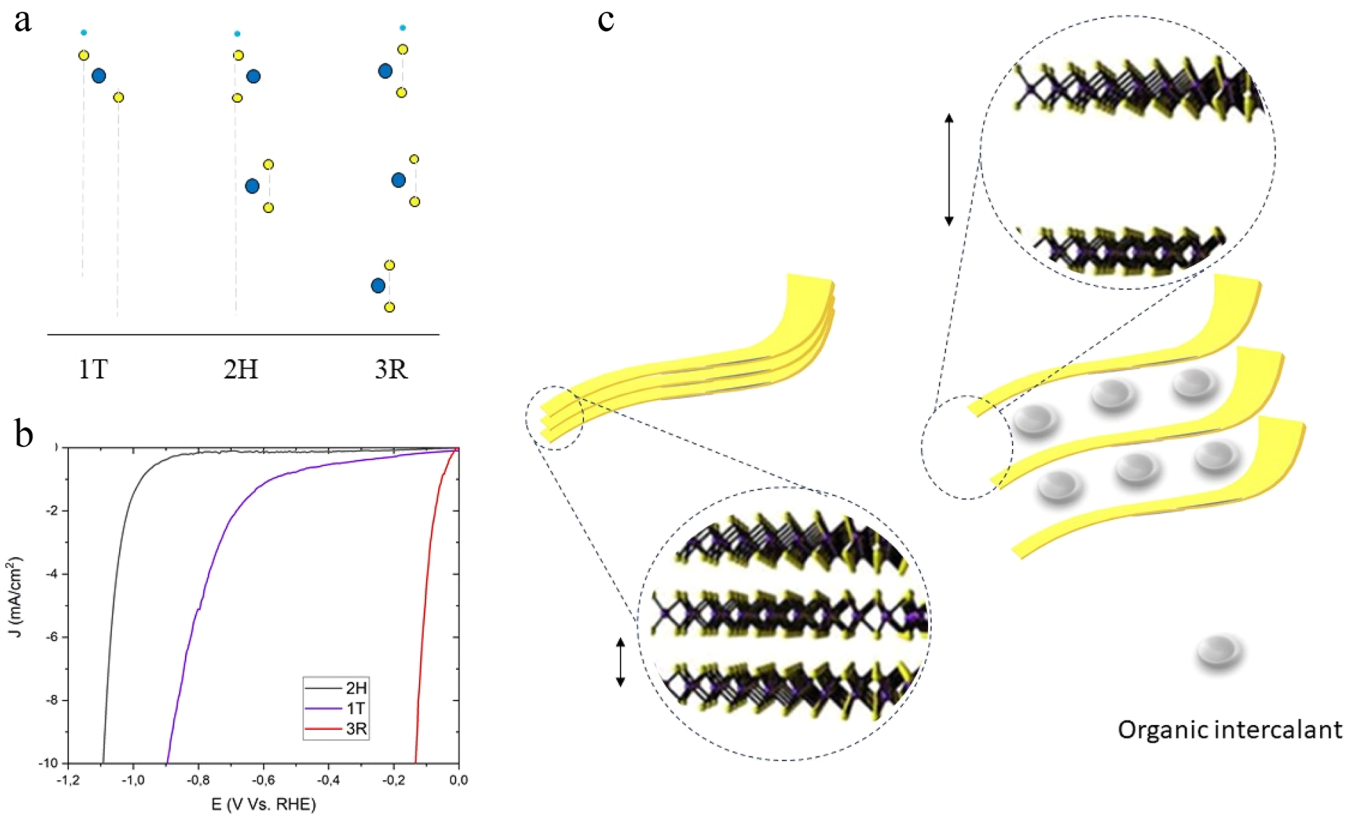

Figure 1. (a) Configuration of sulfur (yellow) and metal (dark blue) for different crystal phases, adsorbed with an H atom (light blue); (b) high-efficiency HER electrocatalysis on 3R TaS_2; and (c) intercalation of the pristine (stacked) nanosheets and increasing of the interlayer space.

calculations that show that a cracked eight-awn star TaS_2 nanostructure possesses significant electrocatalytic properties.[21] They revealed that both basal and edge sites contribute to the HER. Also, Hanlin et al. demonstrated that the electro-exfoliation of bulk TaS_2 into nanosheets can significantly enhance the electrocatalytic activity,[22] leading to a low overpotential and a favorable Tafel slope of 197 mV (@10 $mA{\cdot}cm^{-2}$) and 100 $mV{\cdot}dec^{-1}$, respectively, while compared to those of the parent material (overpotential and Tafel slope of 547 mV and 216 $mV{\cdot}dec^{-1}$, respectively). This demonstrates that the exfoliation of bulk TaS_2 can improve the performance, which may be ascribed to the increase in the interlayer space. Hence, nano-organization of the material is crucial, as it impacts the diffusion of protons via accommodation of more protons at the edge sites where the hot reaction sites are located.

Interestingly, TaS_2 can be exfoliated into nanoflakes, which can host a variety of linear and ring-shaped organic molecules in the interlayer gaps (Figure 1c). To the best of our knowledge, we have not found any prior study reporting the role of intercalated organic molecules on the catalytic efficiency of the HER. In this work, we studied the effect of the intercalation of hexylamine (HA) in TaS_2 nanosheets on the HER performance. The exfoliated TaS_2 nanoflakes were studied with scanning electron microscopy (SEM), and their intercalation with the hexylamine was studied by X-ray diffraction (XRD). The surface compositions were analyzed with X-ray and UV-photoelectron spectroscopies (XPS, UPS). Additional evidence of the structure of the interaction between the organic molecules and exfoliated TaS_2 was obtained by solid-state NMR spectroscopy, and finally, the HER was measured in a standard electrochemical cell.

METHODS

Material Synthesis and Ink Formulation. Tantalum (Ta) and sulfur (S) powders were purchased from Goodfellow, while hexylamine (HA, $C_6H_{15}N$) was bought from Sigma-Aldrich. Ta and S were mixed in a stoichiometric ratio in an agate mortar and then transferred to quartz ampule through a funnel. The ampule was evacuated and flame-sealed. Later, it was placed in a vertical furnace for 48 h at 900 °C and then quenched in water at room temperature. The ampule was opened inside a N_2 glovebox, and the powder was passed through a 125 μm mesh. The powder was heated to 650 °C under vacuum to produce the 3R-TaS_2 crystal structure with an electrical conductivity (σ) of 500 S/cm. HA and TaS_2 were then mixed in a 20:1 molar ratio inside a sealed glass bottle and stirred at 50 °C for 5 days. To suppress the agglomerated particles, the inks of the electrocatalysts were subjected to ultrasonication just before the casting of the films.

Structural Characterization. The X-ray diffraction (XRD) patterns were collected at room temperature using a D8 Bruker diffractometer equipped with a copper anode and a point detector. The scanning electron microscopy (SEM) investigations were carried out with a Hitachi S-4700 equipped with a field emission gun. For both XRD (Bruker D8 Advance/copper/theta-2theta mode/5°−67°/step 0.04°/time: 10 s per step) and SEM (5.00 kV and 12.5*2.50k SE(M) and 10.0 kV and 13.2*5.00k SE(M) for top view and cross section images, respectively) analyses, the TaS_2 powders were drop-casted on glass substrates which were heated at 100 °C for 30 min inside a glovebox to evaporate ethanol used as a solvent.

XPS/UPS (X-ray, ultraviolet photoemission spectroscopy) measurements have been performed in a Scienta ESCA 200

https://doi.org/10.1021/acs.jpcc.2c04290
J. Phys. Chem. C 2022, 126, 17056−17065

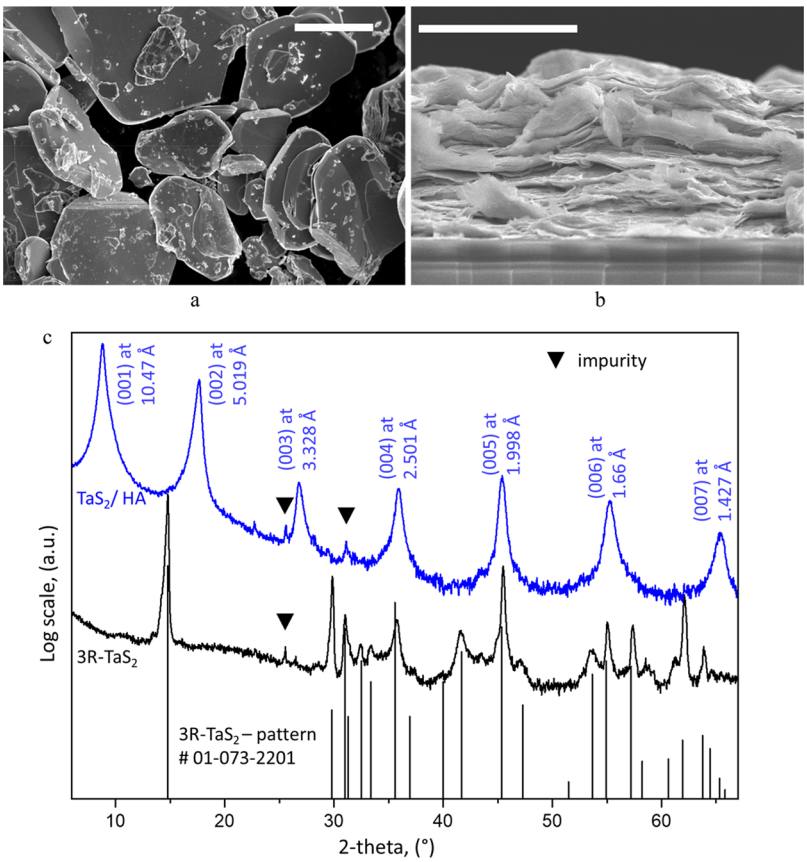

Figure 2. SEM images of TaS_2: (a) top view of the bulk powder and (b) cross section of the film with TaS_2 and HA. The scale bar is 10 μm long. (c) XRD patterns collected on a pristine TaS_2 powder indexed with 01-089-2756 (in black) and TaS_2 intercalated with hexylamine.

system under the base pressure of 2×10^{-10} mbar with an SES 200 electron analyzer, a monochromatic Al Ka X-ray source ($h\upsilon$ = 1486.6 eV), and a helium discharge lamp ($h\upsilon$ = 21.22 eV) for XPS and UPS, respectively. All spectra were collected at normal emission and at room temperature. The spectrometer was calibrated by a sputter-cleaned Au film with the Fermi level at 0 eV and Au 4f7/2 peak at 84.0 eV with its full width at half-maximum being 0.65 eV for XPS. The total energy resolution of UPS is about 0.08 eV estimated from the width of the Fermi edge of a clean Au film. The work function of the sample was extracted from the edge of the secondary electron cutoff in the UPS spectrum with a bias of −3 V applied in the sample.

NMR experiments were recorded on a Bruker Avance 400 III HD spectrometer operating at magnetic fields of 9.4 T. Samples were packed into 2.5 mm zirconia rotors under argon inside a glovebox. The rotors were spun between 10 and 15 kHz at 295 K. ^{1}H MAS were performed with the DEPTH pulse sequence and a recycle delay of 3 s. ^{13}C MAS and CP-MAS were recorded with recycle delays of 5 and 1.5 s, respectively, and with a contact time of 2 ms for CP-MAS. Chemical shifts were externally referenced to liquid TMS. The NMR experiments had to be realized in small rotors (2.5 mm) because of the unfavorable electromagnetic properties of the samples.

Electrochemical Characterization. Electrochemical measurements were carried out using a three-electrode setup (BioLogic SP200 potentiostat) in a 0.5 M H_2SO_4 solution. Graphite felt was used as a counter electrode to provide the highest possible surface area and to avoid any metallic contamination.[23] The structure and performance of carbon felt were characterized and proved during measurement. An Ag/AgCl electrode and a rotating glassy carbon disk electrode were used as a reference electrode and a working electrode, respectively. A 5 wt % Nafion was used as a proton-conductive binder. The measurements were done in the electrolyte where the working electrode was rotating at 800 rpm and the system was purging using pure hydrogen gas. For analysis, all the potentials are converted to a reversible hydrogen electrode using the Nernst equation; in 0.5 M H_2SO_4 (pH = 0), the equation is simplified as E(RHE) = E(SCE) + 0.242.

Linear sweep scan rate (LSV) curves were measured at the scan rate of 5 mV·s^{-1}, in the range of 0.2 to −1 V versus RHE, and all reported values are IR-compensated. The electrochemical active surface area measurements were recorded at scan rates of 10 to 500 mV·s^{-1} in a potential window of 0.14−0.24 (vs RHE).

Results. From the synthesis of TaS_2, we succeeded to obtain a powder of the 3R-TaS_2 crystal structure, which was supported by XRD studies. It was reported[24] that this structurally controlled electrocatalyst showed the highest HER activity in comparison with the other TaS_2 crystal structures illustrated by the lowest overpotential for the HER (0.2 V, compared to 0.47 V for 2H-TaS_2, 0.55 V for 1T-TaS_2 and 0.02 V for Pt) and the lowest Tafel slope of 85 mV/dec (compared to 100 mV/dec for 2H-TaS_2, 155 mV/dec for 1T-TaS_2, and 30 mV/dec for Pt/C). The SEM image of the powder shows platelets of TaS_2 of various sizes (Figure 2a). A compressed layer of this powder displays an electrical conductivity of 500 S/cm suggesting that it has a metallic

https://doi.org/10.1021/acs.jpcc.2c04290
J. Phys. Chem. C 2022, 126, 17056−17065

character. To intercalate HA into the crystal structure, the following simple recipe was used: HA and the TaS_2 powder were mixed in a 20:1 molar ratio inside a sealed glass bottle and stirred at 50 °C for 5 days. That step results in the full intercalation of HA into partially exfoliated TaS_2 nanoflakes.

After exfoliation and intercalation, the suspension was casted on top of a glass substrate to form a thin layer. SEM cross section images, given in Figure 2b, clearly indicate that the thin layers are formed of restacked exfoliated structures oriented parallel to the substrate.

The X-ray diffraction patterns collected on the pristine TaS_2 powder and TaS_2 intercalated with hexylamine are presented in Figure 2c. The XRD pattern obtained from the drop-casted powder has the best match with the ICSD card 01-073-2201[25] that corresponds to 3R-TaS_2 (black pattern). The intercalation of hexylamine into 3R-TaS_2 leads to a superlattice of TaS_2/HA characterized by a series of (00l) peaks where l = 1, 2 up to 7 (blue pattern). Besides strong diffraction from the superlative, some minor peaks are identified as an impurity that could correspond to TaO_x. The comparison of both patterns indicates that the 3R-TaS_2 structure is completely modified by the intercalation of hexylamine as the diffraction from 3R-TaS_2 has entirely vanished on the pattern of the TaS_2/HA.

To better understand the intercalation phenomenon of HA in 3R-TaS_2, the samples were analyzed by X-ray photoelectron spectroscopy (XPS). To emphasize the change in the valency and different chemical environments, all XPS data were plotted with the binding energy relative to the vacuum level. The Ta 4f spectrum of the pristine 3R-TaS_2 clearly indicated that there is more than one type of Ta valency (left panel in Figure 3a). The doublet around 27 and 29 eV is from 3R-TaS_2, where the doublet around 30.5 and 32.5 eV can be attributed to a surface oxide (TaO_x)[26] due to the exposure of 3R-TaS_2 to ambient air. Upon HA intercalation, the Ta 4f doublet from the surface oxide TaO_{5x} can be significantly decreased, which indicates that HA participates in the removal of the oxide. Also meanwhile, it can be clearly seen that the doublet from 3R-TaS_2 has a slight shift to the high binding energy, around 0.3 eV, compared to after HA intercalation. Both features indicate that there is electron transfer from HA to the surface oxide of 3R-TaS_2. Correspondingly, the spectral feature of S 2p (right panel in Figure 3b) from the pristine and HA-treated 3R-TaS_2 shows a decreasing intensity at the high binding energy contribution (ca. 168 eV) and a shift to the low binding energy (ca. 0.2 eV) after HA intercalation. The XPS data clearly indicates that there is a surface chemical reaction present, while the XRD proves that HA is fully intercalated.

We pursue the surface analysis by measuring the UV photoelectron spectra of the samples. A first observation is that the secondary electron cutoff of the UPS spectra (Figure 3c) demonstrates that the work function of 3R-TaS_2 decreases from 4.3 eV, for the pristine air-exposed TaS_2 layer, to 3.9 eV after the intercalation of HA. The drop in work function by 0.4 eV indicates a significant change in the interfacial energetics. The most significant change of the UPS spectra upon HA intercalation is the appearance of the valence features of TaS_2 at 0.5, 1.1, and 2.6 eV relative to the Fermi level (HA has a high valence band feature). On the contrary, there is no visible feature in the pristine 3R-TaS_2, the spectral intensity is very low, and there is almost no feature close to the Fermi level, which is mostly due to the presence of the insulating oxide surface layer with a large energy gap. The surface oxide TaO_x has the dominant contribution to the UPS spectrum of the 3R-

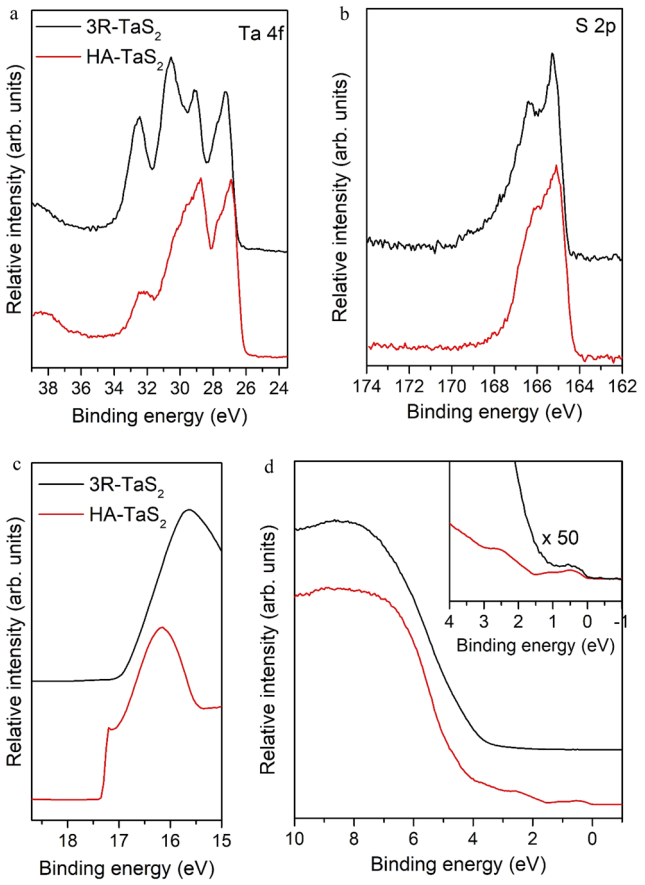

Figure 3. Comparison of the XPS spectra of pristine and HA-intercalated samples: (a) Ta 4f and (b) S 2P. (c) and (d) are the second-electron cutoff and the UPS spectra of pristine and HA-intercalated TaS_2.

TaS_2 surface. Indeed, by zooming in on the energy region close to the Fermi level (inset of Figure 3d), the Fermi edge of the metallic TaS_2 is visible together with the first band at 0.5 eV on the pristine TaS_2 sample. The removal of the surface oxide by the HA treatment leads to an enhancement of about 50 times the valence bands in addition to clear valence band features.

Further insight on the structure of HA interacting with exfoliated TaS_2 was obtained from solid-state NMR spectroscopy. Similar results were obtained regardless of the HA-functionalized TaS_2 batch suggesting that the synthesis is reliable and reproducible. The ^{1}H MAS spectrum of TaS_2 alone displays a weak and broad signal centered at 3 ppm that can be tentatively assigned to isolated hydroxyl groups and physisorbed water molecules (Figure 4a bottom). The ^{1}H MAS spectrum of HA-intercalated TaS_2 (Figure 4a top) shows stronger signals with a characteristic alkyl chain peak at 1.24 ppm and a shoulder at 7.24 ppm attributable to ammonium. This assignment is confirmed by signal deconvolution (Figure S2), with a ratio between the 7.24 and 1.24 signals equal to 0.18 (±0.03), that corresponds to the expected value of 0.2 (3/15, $(NH_3^+)/C_6H_{15}$) for the ammonium species. The ^{13}C CPMAS and MAS spectra (Figure 4b) show broad peak characteristics of disordered structures. The alkylamines adopt several different conformations with varying coordination modes. The ^{13}C CPMAS and MAS spectra are very similar to a good sensitivity of the CP MAS experiment indicating that the amines are rigid in the material.[27] The position of the

https://doi.org/10.1021/acs.jpcc.2c04290
J. Phys. Chem. C 2022, 126, 17056−17065

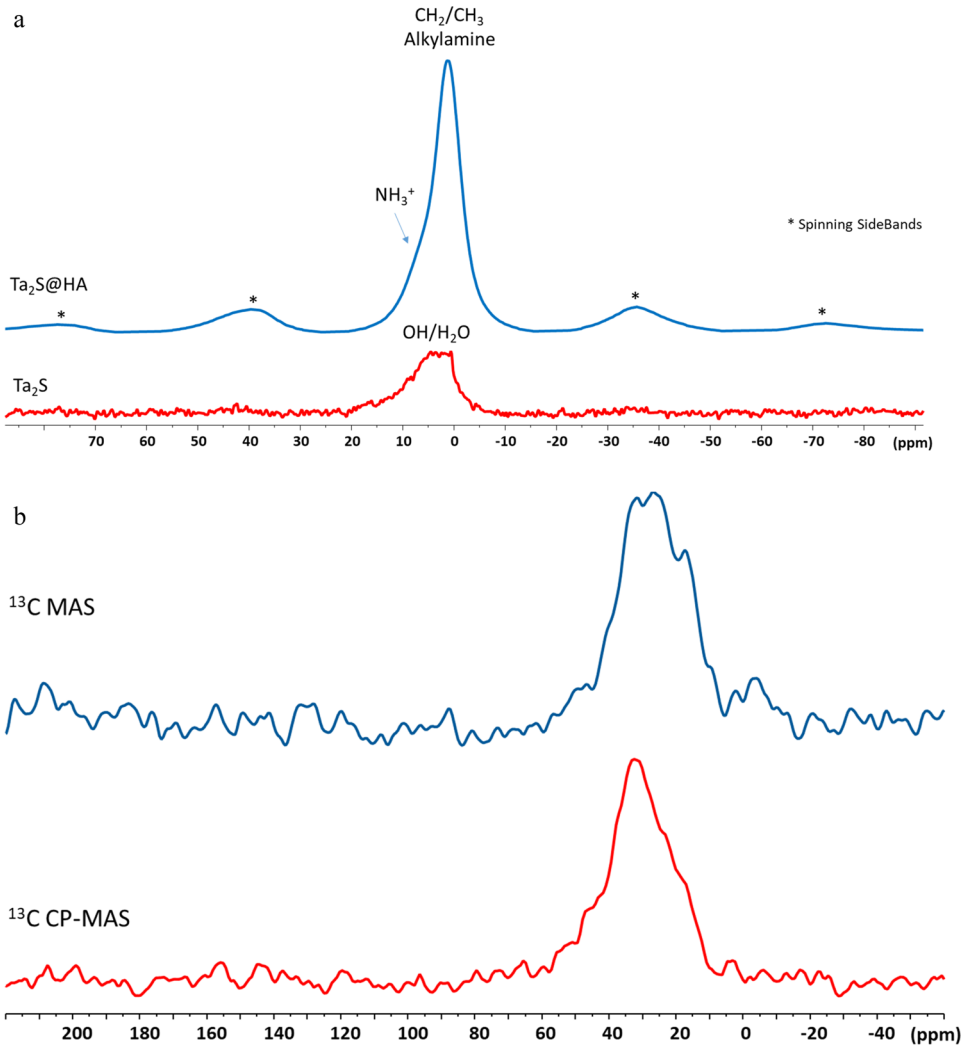

Figure 4. a) ^{1}H MAS spectrum of HA-intercalated TaS_2 and pristine TaS_2. A closer view clearly expresses the fingerprint of the ammonium species; see the deconvoluted spectra (Figure S2). b) ^{13}C CP MAS and ^{13}C MAS spectra of HA-intercalated TaS_2.

central CH_2 groups of the alkyl chain around 30 ppm indicates that the aliphatic chain of the amines is in the form of rigid pellets. Indeed, methylene C atoms with trans/gauche or gauche−gauche conformations exhibit signals at 29−31 ppm (γ-gauche effects), while for all-trans conformations, signals are observed at 33−34 ppm.[28]

Finally, we investigate the electrocatalytic performance of TaS_2 with and without HA intercalation for both the hydrogen evolution reaction (HER) and the hydrogen oxidation reaction (HOR) in an acidic medium. The electrode is prepared in the following way: the TaS_2 powder or the HA-TaS_2 nanoflakes are dispersed in an ethanol−water solution and mixed with 5 wt % of Nafion as a binder, followed by a final deposition on a glassy carbon substrate. We have chosen Nafion as the binder as it is not soluble in water and is also stable in acids. Moreover, it promotes the transport for protons inside the TaS_2 electrode layer, in humid/aqueous conditions. The linear sweep voltammetry visualizes a strong HER activity on the pristine 3R-TaS_2 (Figure 5a). The potentials are referred to as the zero-voltage corresponding to the thermodynamically dictated electronic energy threshold (reversible potential) of the reaction:

$$H^+ + e^- \leftrightarrow H^0 \quad (1)$$

The zero voltage demarcates the potentials of the HER and the HOR manifested in the reversible hydrogen electrode (RHE). The increase in electronic energy, which corresponds to the application of the negative electric potential, beyond a threshold (so-called overpotential) prioritizes reaction 1 from left to right, i.e., the HER. The overpotential for our 3R-TaS_2/Nafion electrode is as low as 0.016 V at the onset. We speculate that the negatively charged Nafion might lead to a small interfacial potential drop with respect to the electrolyte. So, the overpotential is very small, and the HER-driven current rise is remarkable all through −70 mA cm^{-2}, at −0.08 mV, illustrating a diffusion-free behavior typical for fast proton transport. This impressive performance shows that the 3R-TaS_2/Nafion electrode is competitive with other state-of-the-art electrocatalysts for the HER. In contrast, the HA-TaS_2/Nafion electrode with HA intercalation leads to a significantly higher overpotential to observe the onset of the HER and a current level of −7 mA cm^{-2} at −0.34 V, which is significantly smaller than with the TaS_2/Nafion electrode. Note that the blank current collector (glassy carbon) shows an overpotential of ca. 0.74 V, thus demonstrating that it has no impact on the current observed for the TaS_2-based electrodes deposited on glassy carbon.

https://doi.org/10.1021/acs.jpcc.2c04290
J. Phys. Chem. C 2022, 126, 17056−17065

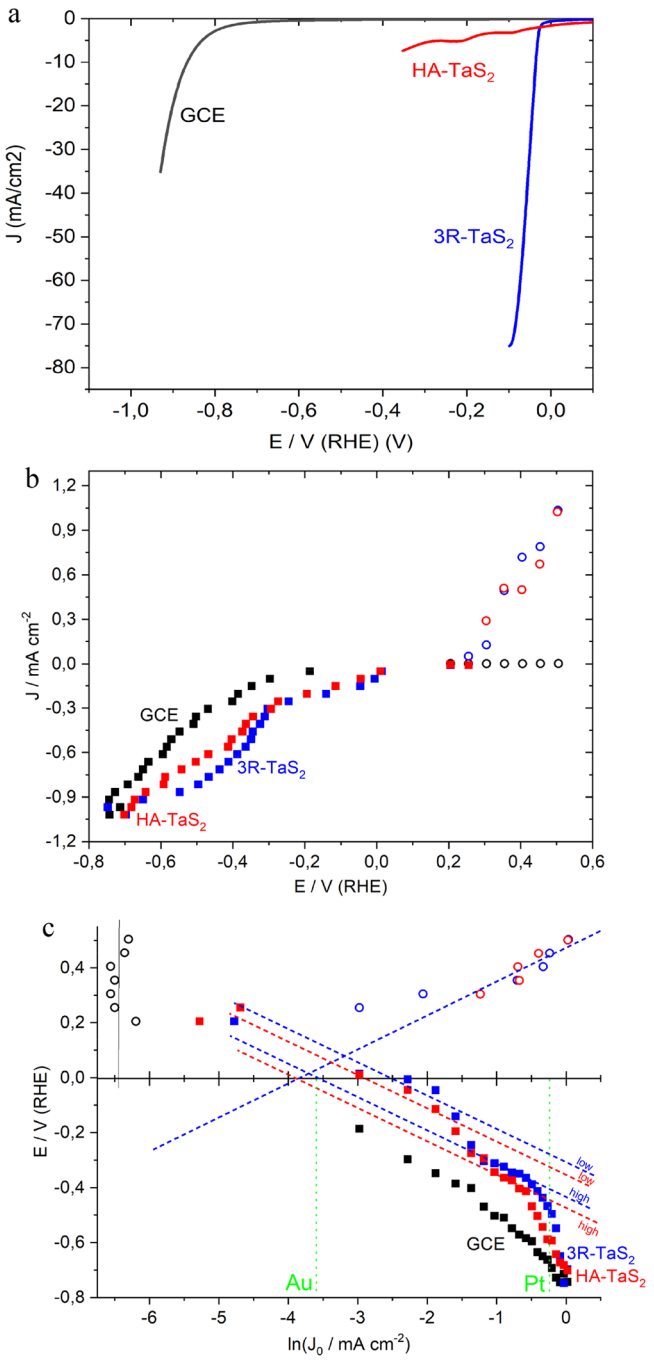

Figure 5. HER/HOR electrocatalysis on TaS_2. Linear sweep (a, 5 mV s^{-1}) and steady-state (b, waiting time of 5 min) voltammograms recorded on blank (ν) and film-modified glassy carbon (pristine and intercalated TaS_2 as blue and red, respectively) and (c) a Tafel plot for the steady-state voltammetry data (filled and hollow symbols refer to the HER and the HOR, respectively; dashed lines—extrapolated Tafel regions); hydrogen-saturated 0.5 M H_2SO_4.

The application-relevant steady-state measurements (Figures 5b and 5c) confirm the increase in the HER rate on the TaS_2 electrode in comparison with the HA intercalated electrode. Importantly, the steady-state measurements allow for the observation of the HOR currents corresponding to the proceeding of reaction 1 running from right to left. The data presentation in Tafel coordinates (Figure 5c) enables us to investigate in detail the electrocatalytic phenomena of the HER and the HOR. In contrast to the smooth glassy carbon electrode, both TaS_2-based electrodes showed nonmonotonous dependence of current density on the overpotential of the HER. Specifically, the region of current densities of 0.27 mA cm^{-2} ($\ln(J) \sim -1.3$, Figure 5c) is characterized with the change of the slope. This might illustrate the effect of kinetic limitation by the mass transport on the highly porous electrocatalyst. The low current densities enable the full involvement of the electrocatalyst surface distributed within nanoscale pores, while the higher current densities are characterized by a limitation of reagent or product transport inside the pores. All electrode systems showed a Tafel slope of ca. 120 mV dec^{-1}. This implies that the rate-determining step in the HER on all electrodes of this study is a Volmer step[29]

$$H_3O^+ + e^- + M \leftrightarrow M\cdots H^0 + H_2O \quad (2)$$

where M denotes the surface empty site.

Coherently with linear sweep voltammetry measurements, the HER showed a higher rate of pristine TaS_2 in comparison with the intercalated TaS_2. Interestingly, the HOR current characteristics reveal an insensitivity to the effect of intercalation of HA on the TaS_2 electrodes. Note, however, that the HOR current is much higher than the vanishingly small current level of the glassy carbon collector. Both pristine and intercalated TaS_2-modified electrodes show a change of Tafel slopes from 40 mV dec^{-1} to 120 mV dec^{-1} as current densities increase. This corresponds to the Volmer step as a rate-determining step in the HOR (reaction 2 proceeds from right to left).[29]

The extrapolation of Tafel slopes (120 mV dec^{-1}) for both the HOR and the HER yields the interception point corresponding to the exchange current density of the HOR/HER—overpotential-free rate of the process, where the rates of both the HOR and the HER are equal. In order to take into account the effect of the nanoscale roughness of porous electrocatalysts,[30] we normalized the estimated exchange current densities to the capacitive current densities, which are assumed to represent the electrochemically available surface area (EASA) of the electrode. The HA intercalated TaS_2 electrode shows up to 20 times higher capacitive currents as compared to the pristine material of the same mass load. We identified this difference as due to the exfoliation process taking place upon HA treatment while producing the nanoflakes (Figure 2b). The exchange current densities estimated from the regions of small overpotentials were 0.041 mA cm^{-2} ($\ln(J_0) \sim -3.18$) and 0.033 mA cm^{-2} ($\ln(J_0) \sim -3.39$) for pristine and intercalated TaS_2. The exchange current densities estimated from the high overpotentials, featured with porous mass transport limitations, were 0.025 mA cm^{-2} ($\ln(J_0) \sim -3.68$) and 0.021 mA cm^{-2} ($\ln(J_0) \sim -3.87$) for pristine and intercalated TaS_2, respectively. The exchange current density for blank glassy carbon is significantly smaller (0.0015 mA cm^{-2} ($\ln(J_0) \sim -6.44$)). The kinetic characteristics obtained for TaS_2 are comparable with the rates of the HER/HOR on gold (0.027 mA cm^{-2} ($\ln(J_0) \sim -3.75$)) and significantly smaller than on platinum (0.78 mA cm^{-2} ($\ln(J_0) \sim -0.23$)). The normalized exchanged current densities show a significant poisoning effect of the hexylamine intercalant (Table 1). The rate of the HOR/HER on intercalated TaS_2 was more than 20 times smaller in comparison with pristine samples.

https://doi.org/10.1021/acs.jpcc.2c04290
J. Phys. Chem. C 2022, 126, 17056−17065

Table 1. Kinetic Parameters of the HER/HOR on TaS_2

interface		J_0, mA cm^{-2}		$J_0/J_{capacitive}$	
		small overpotentials	high overpotentials	small overpotentials	high overpotentials
TaS_2	pristine	0.041	0.025	0.041	0.025
	intercalated	0.033	0.021	0.0016	0.0010
glassy carbon (current collector)		0.0015			
gold[31]		0.027			
platinum[32]		0.78			

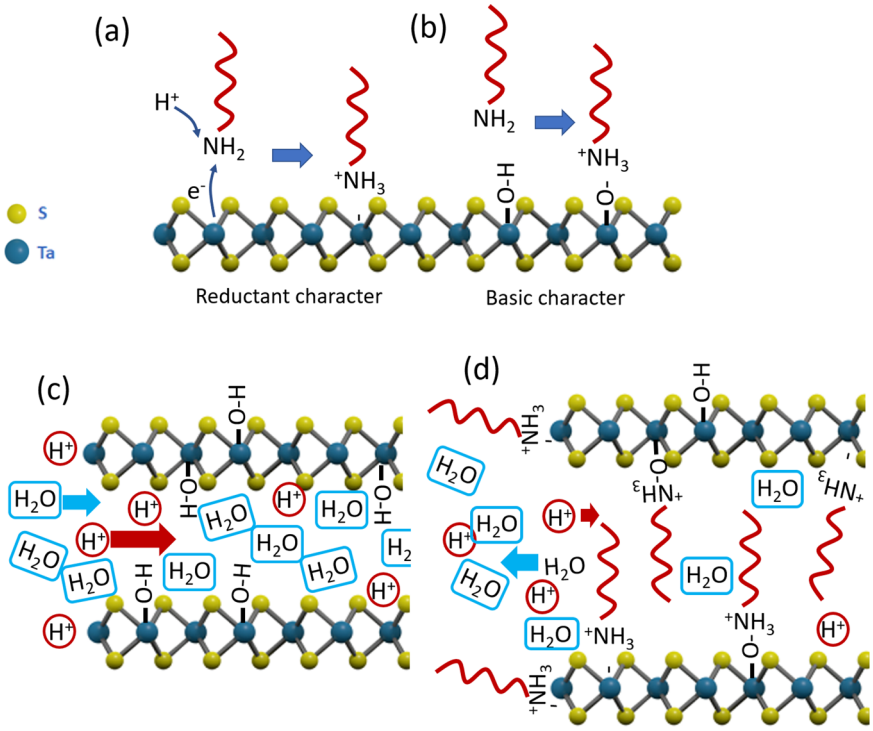

Figure 6. (a) Reductant character of the hexylamine leading to electron transfer and chemical interaction with TaS_2. (b) Basic character of the hexylamine reacting with a hydroxyl surface group on TaS_2. (c) Proton diffusion is promoted in the hydrophilic van der Waals gaps of the TaS_2. (d) Hexylamine intercalation of TaS_2 leads to hydrophobic van der Waals gaps that block the water diffusion and diminish the transport of the proton to catalytic sites.

DISCUSSION

To improve reaction rates, a critical phenomenon of interest is the removal/reduction/dissolution of the Ta_2O_5 surface oxide by the reaction with HA. Alkyl amines are known to serve as reducing agents for metal oxide nanoparticles;[33] hence, we believe that HA reduces TaS_2 not only to functionalize its surface (Figure 6a) but also to remove the surface oxide of TaS_2. Both XPS and UPS results are in agreement with this interpretation. Now, the XRD demonstrates the full intercalation of the HA in the TaS_2; hence, HA not only removes the oxide but truly intercalates in the van der Waals gaps of the TaS_2. Understanding the nature of the surface and edge of the TaS_2 nanoflakes is important to explore the electrocatalytic reactions. The UPS reveals that the metallic electronic structure of TaS_2 (high density of states at the Fermi level) is enhanced after HA treatment as the surface oxide is removed. Thus, one could imagine that the electrocatalytic activity would be boosted thanks to available metallic levels on the surface. However, the electrochemical data tells us the opposite. Indeed, a larger overpotential and lower current densities are obtained for the HER upon HA intercalation. It is thus reasonable to think that the HA molecules are also forming a submonolayer on the surface of the TaS_2 nanoflakes and that its interaction with Ta atoms blocks electrocatalytic reactions. For instance, it is known that HA is forming a monolayer on various 2D materials by a chemical reaction involving hydroxyl groups contaminating their surface in the presence of air and humidity.[34] The mechanism proposed involves the basic character of the amine with a proton transfer from the surface hydroxide groups: Ta−OH + H_2N−R → (Ta−O^-)($^+NH_3$−R) (see Figure 6b). NMR spectroscopic measurements agree with this assumption. It is proved that the resulting formed monolayer can remove water molecules from the van der Waals gaps by expressing its hydrophobic character, which in turn suppresses the nanosheet catalytic activity and ion transport toward the HER. The structure of the aliphatic chain of HA in the form of rigid pellets also agreed with the hydrophobic character of the organic layer. The moderate water-blocking property is also demonstrated when similar architectures of graphene oxide are treated with different alkylamines.[35] Moreover, the contact angle of HA-treated TaS_2 nanoflakes is twice those measured on nonsurface modified systems and further increases for longer alkyl chains of the alkylamine.[36]

https://doi.org/10.1021/acs.jpcc.2c04290
J. Phys. Chem. C 2022, 126, 17056−17065

Apart from that, surface charges will remain at the surface of the structure, which shows that the zeta potential of the intercalated TaS_2 likely decreases. This decrement in surface charges has a detrimental effect on the electron transfer between the surface and the protons,[36,37] thus, negatively impressing the HER activity of the electrocatalyst.

Moreover, the intercalation with HA increases the band gap, meaning that the higher overpotential is needed to drive the reaction of hydrogen reduction.[38] In principle, the HA intercalation will increase the interlayer gap between nanosheets.

However, the effect of impurity was not inevitable in this study, as the impurity is detected by the XRD spectrum (Figure 2). We assume that we have some impurity during the synthesis of the electrocatalyst, since the materials were transferred to an ampule and later passed through a mesh. These introduce impurities and possible defects to the film, which may impact the performance of electrocatalysts.[39,40] The optimized effect of defects might enhance the performance of the electrocatalyst, though, as it is already reported in the case of the transitional metal dichalcogenide HER application.[41] The reason is that the optimized level of defects can offer local higher charge density.[42] Although there are some reports regarding the one-spot electrodeposition directly on the electrode,[40] the side deposition of species is not inevitable.

CONCLUSIONS

In summary, 3R-TaS_2 nanosheets and the hexylamine-treated derivative were investigated for hydrogen evolution. The aliphatic intercalant can conduct a high electron donor process of intercalation. XPS and XRD spectroscopy measurements show that the interlayer distance in nanosheets has been increased as a result of hexylamine intercalation. Polarization curves show us an excellent performance of the pristine 3R-TaS_2 sample, while the intercalated sample reveals a deteriorated performance. The suppressing effect of HA-TaS_2 could come from the (i) decrease of the surface charges associated with a decrease in their mobility, (ii) water molecule-blocking, and (iii) bandgap increment, as post-intercalation effects. Apart from that, the hydrogen oxidation measurements express that both catalysts are quite active for the reverse reaction when hydrogen is oxidized, converted to electricity. While the current density for the catalyst exponentially increases as the potential increases, glassy carbon does not show any potential dependency and stays at the current density of 0 V. Tafel slopes also show the Volmer reaction as the rate-determining step for both evolution and oxidation of hydrogen. This work demonstrates TaS_2 nanosheets as a versatile electrified interface, which can be used either as an efficient HER/HOR electrocatalyst or as an inert current collector.

ASSOCIATED CONTENT

Supporting Information

The Supporting Information is available free of charge at https://pubs.acs.org/doi/10.1021/acs.jpcc.2c04290.

Cyclic voltammograms and ^{1}H MAS spectrum (PDF)

AUTHOR INFORMATION

Corresponding Authors

Hamid Ghorbani Shiraz − *Laboratory of Organic Electronics, Department of Science and Technology, Linköping University, Norrköping SE-60174, Sweden;* orcid.org/0000-0002-2001-1538; Email: Hamid.ghorbani.shiraz@liu.se

Mikhail Vagin − *Laboratory of Organic Electronics, Department of Science and Technology, Linköping University, Norrköping SE-60174, Sweden*; Email: mikhail.vagin@liu.se

Authors

Zia Ullah Khan − *Laboratory of Organic Electronics, Department of Science and Technology, Linköping University, Norrköping SE-60174, Sweden*

Daniel Péré − *Department of Advanced Materials, IMRA Europe S.A.S., 06904 Sophia Antipolis, France*

Xianjie Liu − *Laboratory of Organic Electronics, Department of Science and Technology, Linköping University, Norrköping SE-60174, Sweden;* orcid.org/0000-0002-3190-2774

Yannick Coppel − *LCC-CNRS, University of Toulouse, CNRS, 31400 Toulouse, France;* orcid.org/0000-0003-0970-4082

Mats Fahlman − *Laboratory of Organic Electronics, Department of Science and Technology, Linköping University, Norrköping SE-60174, Sweden;* orcid.org/0000-0001-9879-3915

Magnus Berggren − *Laboratory of Organic Electronics, Department of Science and Technology, Linköping University, Norrköping SE-60174, Sweden;* orcid.org/0000-0001-5154-0291

Radoslaw Chmielowski − *Department of Advanced Materials, IMRA Europe S.A.S., 06904 Sophia Antipolis, France*

Myrtil L. Kahn − *LCC-CNRS, University of Toulouse, CNRS, 31400 Toulouse, France;* orcid.org/0000-0003-3079-5759

Xavier Crispin − *Laboratory of Organic Electronics, Department of Science and Technology, Linköping University, Norrköping SE-60174, Sweden;* orcid.org/0000-0001-8845-6296

Complete contact information is available at: https://pubs.acs.org/10.1021/acs.jpcc.2c04290

Notes

The authors declare no competing financial interest.

ACKNOWLEDGMENTS

This work was financially supported by the Swedish Research Council (VR 2016-05990), the Knut and Alice Wallenberg Foundation (KAW 2019.0604; 2021.0195), the Karl Erik Önnesjös Foundation, and the Swedish Government Strategic Research Area in Materials Science on Advanced Functional Materials at Linköping University (Faculty Grant SFO-Mat-LiU No. 2009-00971).

REFERENCES

(1) Jin, T. L.; Liu, X.; Wang, H.; Wu, X.; Zhang, Y. Mechanochemical-Assisted Synthesis of Ternary Ru-Ni-S Pyrite Analogue for Enhanced Hydrogen Evolution Performance. *Carbon* **2020**, *162*, 172−180.

(2) Suliman, M. H.; Adam, A.; Li, L.; Tian, Z.; Siddiqui, M. N.; Yamani, Z. H.; Qamar, M. Fep/Mos2 Enriched with Dense Catalytic Sites and High Electrical Conductivity for the Hydrogen Evolution Reaction. *ACS Sustainable Chem. Eng.* **2019**, *7*, 17671−17681.

(3) Bai, S.; Wang, C.; Deng, M.; Gong, M.; Bai, Y.; Jiang, J.; Xiong, Y. Surface Polarization Matters: Enhancing the Hydrogen-Evolution Reaction by Shrinking Pt Shells in Pt-Pd-Graphene Stack Structures. *Angew. Chem.* **2014**, *126*, 12316−12320.

(4) Yan, X.; Tian, L.; He, M.; Chen, X. Three-Dimensional Crystalline/Amorphous Co/Co3o4 Core/Shell Nanosheets as Efficient Electrocatalysts for the Hydrogen Evolution Reaction. *Nano Lett.* **2015**, *15*, 6015−6021.
(5) Luo, X.; Zhou, Q.; Du, S.; Li, J.; Zhang, L.; Lin, K.; Li, H.; Chen, B.; Wu, T.; Chen, D. One-Dimensional Porous Hybrid Structure of Mo2c-Cop Encapsulated in N-Doped Carbon Derived from Mof: An Efficient Electrocatalyst for Hydrogen Evolution Reaction over the Entire Ph Range. *ACS Appl. Mater. Interfaces* **2018**, *10*, 42335−42347.
(6) Lin, Y.; Zhang, M.; Zhao, L.; Wang, L.; Cao, D.; Gong, Y. Ru Doped Bimetallic Phosphide Derived from 2d Metal Organic Framework as Active and Robust Electrocatalyst for Water Splitting. *Appl. Surf. Sci.* **2021**, *536*, 147952.
(7) Zhu, Y.; Lin, Q.; Zhong, Y.; Tahini, H. A.; Shao, Z.; Wang, H. Metal Oxide-Based Materials as an Emerging Family of Hydrogen Evolution Electrocatalysts. *Energy Environ. Sci.* **2020**, *13*, 3361−3392.
(8) Dunnill, C. W.; MacLaren, I.; Gregory, D. H. Superconducting Tantalum Disulfide Nanotapes; Growth, Structure and Stoichiometry. *Nanoscale* **2010**, *2*, 90−97.
(9) Geng, S.; Yang, W.; Liu, Y.; Yu, Y. Engineering Sulfur Vacancies in Basal Plane of Mos2 for Enhanced Hydrogen Evolution Reaction. *J. Catal.* **2020**, *391*, 91−97.
(10) Voiry, D.; Salehi, M.; Silva, R.; Fujita, T.; Chen, M.; Asefa, T.; Shenoy, V. B.; Eda, G.; Chhowalla, M. Conducting Mos2 Nanosheets as Catalysts for Hydrogen Evolution Reaction. *Nano Lett.* **2013**, *13*, 6222−6227.
(11) Li, Y.; Wang, H.; Xie, L.; Liang, Y.; Hong, G.; Dai, H. Mos2 Nanoparticles Grown on Graphene: An Advanced Catalyst for the Hydrogen Evolution Reaction. *J. Am. Chem. Soc.* **2011**, *133*, 7296−7299.
(12) Yu, Y.; Huang, S.-Y.; Li, Y.; Steinmann, S. N.; Yang, W.; Cao, L. Layer-Dependent Electrocatalysis of Mos2 for Hydrogen Evolution. *Nano Lett.* **2014**, *14*, 553−558.
(13) Bulaevskiĭ, L. Structural Transitions with Formation of Charge-Density Waves in Layer Compounds. *Soviet Physics Uspekhi* **1976**, *19*, 836.
(14) Gamble, F.; Osiecki, J. H.; Cais, M.; Pisharody, R.; DiSalvo, F.; Geballe, T. Intercalation Complexes of Lewis Bases and Layered Sulfides: A Large Class of New Superconductors. *Science* **1971**, *174*, 493−497.
(15) Gamble, F.; DiSalvo, F.; Klemm, R.; Geballe, T. Superconductivity in Layered Structure Organometallic Crystals. *Science* **1970**, *168*, 568−570.
(16) Zhang, X.; Fei, H.; Wu, Z.; Wang, D. A Facile Preparation of Ws2 Nanosheets as a Highly Effective Her Catalyst. *Tungsten* **2019**, *1*, 101−109.
(17) Li, H.; Tan, Y.; Liu, P.; Guo, C.; Luo, M.; Han, J.; Lin, T.; Huang, F.; Chen, M. Atomic-Sized Pores Enhanced Electrocatalysis of Tas2 Nanosheets for Hydrogen Evolution. *Adv. Mater.* **2016**, *28*, 8945−8949.
(18) Wu, J.; Liu, M.; Chatterjee, K.; Hackenberg, K. P.; Shen, J.; Zou, X.; Yan, Y.; Gu, J.; Yang, Y.; Lou, J. Exfoliated 2d Transition Metal Disulfides for Enhanced Electrocatalysis of Oxygen Evolution Reaction in Acidic Medium. *Advanced Materials Interfaces* **2016**, *3*, 1500669.
(19) Wang, X.; Wang, D.; Lu, Y.; Song, C.; Pan, J.; Li, C.; Sui, M.; Zhao, W.; Huang, F. In Atom-Scale Dispersed Palladium in a Conductivepd0.1tas2 Lattice with a Unique Electronic Structure for Efficient Hydrogen Evolution; *ECS Meeting Abstracts*; IOP Publishing: 2020; p 2434.
(20) Yu, Q.; Luo, Y.; Qiu, S.; Li, Q.; Cai, Z.; Zhang, Z.; Liu, J.; Sun, C.; Liu, B. Tuning the Hydrogen Evolution Performance of Metallic 2d Tantalum Disulfide by Interfacial Engineering. *ACS Nano* **2019**, *13*, 11874−11881.
(21) Feng, Y.; Yu, K.; Zhu, Z. Cracked Eight-Awn Star Tas 2 with Fractal Structures Used as an Efficient Electrocatalyst for the Hydrogen Evolution Reaction. *CrystEngComm* **2019**, *21*, 3517−3524.
(22) Chen, H.; Si, J.; Lyu, S.; Zhang, T.; Li, Z.; Lei, C.; Lei, L.; Yuan, C.; Yang, B.; Gao, L. Highly Effective Electrochemical Exfoliation of Ultrathin Tantalum Disulfide Nanosheets for Energy-Efficient Hydrogen Evolution Electrocatalysis. *ACS Appl. Mater. Interfaces* **2020**, *12*, 24675−24682.
(23) Gu, C.; Norris, B. C.; Fan, F.-R. F.; Bielawski, C. W.; Bard, A. J. Is Base-Inhibited Vapor Phase Polymerized Pedot an Electrocatalyst for the Hydrogen Evolution Reaction? Exploring Substrate Effects, Including Pt Contaminated Au. *ACS Catal.* **2012**, *2*, 746−750.
(24) Feng, Y.; Gong, S.; Du, E.; Chen, X.; Qi, R.; Yu, K.; Zhu, Z. 3r Tas2 Surpasses the Corresponding 1t and 2h Phases for the Hydrogen Evolution Reaction. *J. Phys. Chem. C* **2018**, *122*, 2382−2390.
(25) Bevan, D.; Martin, R. L.; Vegas, A.Rationalization of the Substructures Derived from the Three Fluorite-Related [Li6 (Mvli) N4] Polymorphs: An Analysis in Terms of the "Bärnighausen Trees" and of the "Extended Zintl-Klemm Concept. In *Inorganic 3d Structures*; Springer: 2011; pp 93−131, DOI: 10.1007/430_2011_39.
(26) Chamlagain, B.; Cui, Q.; Paudel, S.; Cheng, M. M.-C.; Chen, P.-Y.; Zhou, Z. Thermally Oxidized 2d Tas2 as a High-K Gate Dielectric for Mos2 Field-Effect Transistors. *2D Materials* **2017**, *4*, 031002.
(27) Spataro, G.; Champouret, Y.; Coppel, Y.; Kahn, M. L. Prominence of the Instability of a Stabilizing Agent in the Changes in Physical State of a Hybrid Nanomaterial. *ChemPhysChem* **2020**, *21*, 2454−2459.
(28) Spataro, G.; Champouret, Y.; Florian, P.; Coppel, Y.; Kahn, M. L. Multinuclear Solid-State Nmr Study: A Powerful Tool for Understanding the Structure of Zno Hybrid Nanoparticles. *Phys. Chem. Chem. Phys.* **2018**, *20*, 12413−12421.
(29) Shinagawa, T.; Garcia-Esparza, A. T.; Takanabe, K. Insight on Tafel Slopes from a Microkinetic Analysis of Aqueous Electrocatalysis for Energy Conversion. *Sci. Rep.* **2015**, *5*, 13801.
(30) Voiry, D.; Chhowalla, M.; Gogotsi, Y.; Kotov, N. A.; Li, Y.; Penner, R. M.; Schaak, R. E.; Weiss, P. S. Best Practices for Reporting Electrocatalytic Performance of Nanomaterials. *ACS Nano* **2018**, *12*, 9635−9638.
(31) Creţu, R.; Kellenberger, A.; Medeleanu, M.; Vaszilcsin, N. Cathodic Hydrogen Evolution Reaction on Gold Catalyzed by Proton-Carriers. *Int. J. Electrochem. Sci.* **2014**, *9*, 4465−4477.
(32) Nørskov, J. K.; Bligaard, T.; Logadottir, A.; Kitchin, J.; Chen, J. G.; Pandelov, S.; Stimming, U. Trends in the Exchange Current for Hydrogen Evolution. *J. Electrochem. Soc.* **2005**, *152*, J23.
(33) Meffre, A.; Lachaize, S.; Gatel, C.; Respaud, M.; Chaudret, B. Use of Long Chain Amine as a Reducing Agent for the Synthesis of High Quality Monodisperse Iron (0) Nanoparticles. *J. Mater. Chem.* **2011**, *21*, 13464−13469.
(34) Su, C.; Yin, Z.; Yan, Q.-B.; Wang, Z.; Lin, H.; Sun, L.; Xu, W.; Yamada, T.; Ji, X.; Zettsu, N. Waterproof Molecular Monolayers Stabilize 2d Materials. *Proc. Natl. Acad. Sci. U. S. A.* **2019**, *116*, 20844−20849.
(35) Abdullahi, B.; Ahmed, E.; Al Abdulgader, H.; Alghunaimi, F.; Saleh, T. A. Facile Fabrication of Hydrophobic Alkylamine Intercalated Graphene Oxide as Absorbent for Highly Effective Oil-Water Separation. *J. Mol. Liq.* **2021**, *325*, 115057.
(36) Huang, W.-M.; Liao, W.-S.; Lai, Y.-M.; Chen, I.-W. P. Tuning the Surface Charge Density of Exfoliated Thin Molybdenum Disulfide Sheets Via Non-Covalent Functionalization for Promoting Hydrogen Evolution Reaction. *Journal of Materials Chemistry C* **2020**, *8*, 510−517.
(37) Shiraz, H. G.; Crispin, X.; Berggren, M. Transition Metal Sulfides for Electrochemical Hydrogen Evolution. *Int. J. Hydrogen Energy* **2021**, *46*, 24060−24077.
(38) Hunt, A.; Kurmaev, E.; Moewes, A. Band Gap Engineering of Graphene Oxide by Chemical Modification. *Carbon* **2014**, *75*, 366−371.
(39) Toh, R. J.; Sofer, Z.; Luxa, J.; Pumera, M. Ultrapure Molybdenum Disulfide Shows Enhanced Catalysis for Hydrogen Evolution over Impurities-Doped Counterpart. *ChemCatChem.* **2017**, *9*, 1168−1171.
(40) Strange, L. E.; Garg, S.; Kung, P.; Ashaduzzaman, M.; Szulczewski, G.; Pan, S. Electrodeposited Transition Metal

Dichalcogenides for Use in Hydrogen Evolution Electrocatalysts. *J. Electrochem. Soc.* **2022**, *169*, 026510.
(41) Wang, J.; Liu, J.; Zhang, B.; Ji, X.; Xu, K.; Chen, C.; Miao, L.; Jiang, J. The Mechanism of Hydrogen Adsorption on Transition Metal Dichalcogenides as Hydrogen Evolution Reaction Catalyst. *Phys. Chem. Chem. Phys.* **2017**, *19*, 10125−10132.
(42) Jia, Y.; Zhang, L.; Gao, G.; Chen, H.; Wang, B.; Zhou, J.; Soo, M. T.; Hong, M.; Yan, X.; Qian, G. A Heterostructure Coupling of Exfoliated Ni-Fe Hydroxide Nanosheet and Defective Graphene as a Bifunctional Electrocatalyst for Overall Water Splitting. *Adv. Mater.* **2017**, *29*, 1700017.

https://doi.org/10.1021/acs.jpcc.2c04290
J. Phys. Chem. C 2022, 126, 17056−17065